Separation and Purification Technology 290 (2022) 120786

Contents lists available at ScienceDirect

Separation and Purification Technology

journal homepage: www.elsevier.com/locate/seppur

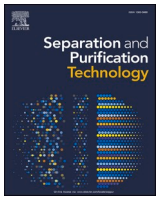

CO_2 absorption into aqueous ammonia using membrane contactors: Role of solvent chemistry and pore size on solids formation for low energy solvent regeneration

S. Bavarella [a], B. Luqmani [a], N. Thomas [a], A. Brookes [b], A. Moore [c], P. Vale [d], M. Pidou [a], E. J. McAdam [a,*]

[a] Cranfield Water Science Institute, Vincent Building, Cranfield University, Bedfordshire MK43 0AL, UK
[b] Anglian Water, Block C-Western House, Peterborough Business Park, Lynch Wood, Peterborough PE2 6FZ, UK
[c] Northumbrian Water, Boldon House, Wheatlands Way, Durham DH1 5FA, UK
[d] Severn Trent Water, 2 St. Johns Street, Coventry CV1 2LZ, UK

ARTICLE INFO

Keywords:
Chilled ammonia
Carbon capture and storage (CCS)
Membrane crystallisation
Ammonium bicarbonate solid formation
Ammonium bicarbonate crystallisation/ precipitation

ABSTRACT

Solids formation can substanitally reduce the energy penalty for ammonia solvent regeneration in carbon capture and storage (CCS), but has been demonstrated in the literature to be difficult to control. This study examines the use of hollow fibre membrane contactors, as this indirect contact mediated between liquid and gas phases in this geometry could improve the regulation of solids formation. Under conditions comparable to existing literature, NH_4HCO_3 was evidenced to primarily crystallise in the gas-phase (lumen-side of the membrane) due to the high vapour pressure of ammonia, which promotes gaseous transmission from the solvent. Investigation of solvent reactivity demonstrated how equilibria dependent reactions controlled the onset of NH_4HCO_3 nucleation in the solvent, and limited 'slip' through transfomation of ammonia into its protonated form which occurs prior to the phase change. Crystallisation in the solvent was also dependent upon ammonia concentration, where sufficient supersaturation must develop to overcome the activation energy for nucleation. However, this has to be complemented with a reduction in solvent temperature to offset vapour pressure and limit the risk of gas-phase crystallisation. While changes to the solvent chemistry were sufficient to shift from gas-phase to liquid phase crystallisation, wetting was observed immediately after nucleation in the solvent. This was explained by a local region of supersaturation within the coarse membrane pores that promoted a high nucleation rate, altering the material contact angle of the membrane sufficient for solvent to breakthrough into the gas phase. Adoption of a narrower pore size membrane was shown to dissipate wetting after crystallisation in the solvent, illustrating membrane contactors as a stable platform for the sustained separation of CO_2 coupled with its simultaneous transformation into a solid. Through resolving previous challenges experienced with solids formation in multiple reactor configurations, the cost benefit of using ammonia as a solvent can be realised, which is critical to enabling economically viable CCS for the transition to net zero, and can be exploited within hollow fibre membrane contactors, eliciting considerable process intensification over existing reactor designs for CCS.

1. Introduction

Carbon capture and storage (CCS) is expected to play a critical role in the transition to net zero. The use of ammonia (NH_3) as a reactive solvent for the selective separation of carbon dioxide (CO_2) has been demonstrated to achieve absorption capacities three times higher than sterically free primary alkanolamines, which is critical to driving down the cost barrier for CCS [43]. Control of the overall reaction can lead to the formation of solid (crystalline) ammonium bicarbonate (NH_4HCO_3) as the final product [2]. This can reduce the mass flow of stripping solution, lowering the thermal demand for regeneration, and therefore further benefitting the separation costs for CCS [36]. Formation of crystalline NH_4HCO_3 through reactive absorption of CO_2 has therefore been studied in conventional packed column absorbers, where solids formation has also been shown to limit NH_3 'slip' into the gas phase, therefore eliminating the need for gas-phase abatement technology

* Corresponding author.
E-mail address: e.mcadam@cranfield.ac.uk (E.J. McAdam).

https://doi.org/10.1016/j.seppur.2022.120786
Received 26 January 2022; Received in revised form 3 March 2022; Accepted 4 March 2022
Available online 12 March 2022

Table 1
Literature review of ammonia-CO_2 absorption in hollow fibre membrane contactors where crystallisation has been observed.

Ref.	Operating conditions				Absorbent				Feed gas				Ammonium Bicarbonate crystallisation observed
	Membrane/ ID (mm)[b]	Pore size (μm)	Gas CSA[c] (x10^6 m^2)	Liquid flow/ Gas side	$[NH_3]$[d] (mol L^{-1})	C*[a] (mol L^{-1})	pH -	T[e] (°C)	$[CO_2]$/ RH_{inlet} (%)	T[e] (°C)	Gas velocity (m s^{-1})	Liquid velocity (x10^3 m s^{-1})	
[24]	PP/0.3	0.2	0.07	S.P. [f] / lumen	0.6–2.9	2.4 ± 0.2	>11	21	15/0	21	0.4–1.1	0.086–0.24	Gas side
[26]	PTFE/1.5	–	1.8	Recycle / lumen	2	2.4 ± 0.2	>11	20	50/0	20	0.93	20	Liquid side
	PTFE/1.5	–	1.8	Recycle / lumen	3–5	2.4 ± 0.2	>11	20	50/0	20	0.93	20	Gas side
[9]	PTFE/1.5	2.6	450	S.P. [f] / shell	1–3.7	2.4 ± 0.2	>11	21	10–15-20/0	21	0.11	5–40	Gas side
[40]	PP + PMP/0.2	–	0.03	S.P. [f] / lumen	2.9	1.9 ± 0.1	>11	10	15/100	10	2	2	Gas side
	PP + PMP/0.2	–	0.03	S.P. [f] / lumen	2.9	1.9 ± 0.1	>11	10	15/0	10	2	2	Gas side
	PP + PMP/0.2	–	0.03	S.P. [f] / lumen	2.9	2.4 ± 0.2	>11	21	15/100	21	2	2	Gas side
	PP + PMP/0.2	–	0.03	S.P. [f] / lumen	2.9	2.4 ± 0.2	>11	21	15/0	21	2	2	Gas side
	PP + PMP/0.2	–	0.03	S.P. [f] / lumen	2.9	2.4 ± 0.2	>11	21	15/0	21	1.3	2	Gas side
	PP + PMP/0.2	–	0.03	S.P. [f] / lumen	2.9	2.4 ± 0.2	>11	21	15/100	21	1.3	2	Gas side
	PP + PMP/0.2	–	0.03	S.P. [f] / lumen	2.9	3.8	>11	40	15/0	40	1.3	2	Not observed
This study	PP/1.2	0.36–0.2	1.1	Recycle / lumen	3	1.6 ± 0.1	10	5	100/0	20	14.7	60	Liquid side
	PTFE/2.4	3.4–0.5	4.5	Recycle / lumen	3	1.6 ± 0.1	10	5	100/0	20	3.7	60	Liquid side
	PTFE/2.4	3.4–0.5	4.5	S.P. [f] / lumen	2.3–3	2.4 ± 0.2	>11	20	100/0	20	0.2	1.4	Gas side

[a] Ammonia concentration at supersaturation for given absorbent temperature [31,38,33],[b]ID, Inner diameter; [c]CSA, Cross sectional area; [d]$[NH_3]$, Ammonia concentration; [e]T, Temperature; [f]SP, Single pass.

Table 2
Dimensions and surface characteristics of the single membrane fibre.

		PP	PTFE
Fibre characteristics			
Membrane material	–	Polypropylene (PP)	Polytetrafluoroethylene (PTFE)
Inner diameter	mm	1.2	2.4
Outer diameter	mm	1.8	2.8
Wall thickness	μm	300	200
Active length	mm	165	165
Surface area[bb]	m^2_b	9.33×10^{-4}[b]	1.44×10^{-3}[b]
Porosity	%	72 ± 2[a]	60 ± 10[a]
ΔG_{het} / ΔG_{hom}	%	60	90
Minimum pore size, (d_{min})	μm	0.2[a]	0.18[c]
Maximum pore size, (d_{max})	μm	0.36[c]	4.5[c]
Geometrical factor, B	–	0.56	0.15
Contact angle, (θ)	°	117[db]	135[db]
Breakthrough pressure, ($\Delta P_{B.P.}$)	bar	2.0[eb]	0.3[e]
Lumen cross sectional area	m^2[b]	1.13×10^{-6}[b]	4.5×10^{-6}[b]
Shell side characteristics			
Height	mm	5	5
Width	mm	12	12
Shell cross sectional area	m^2[b]	6.0×10^{-5}[b]	6.0×10^{-5}[b]
Priming volume	ml	11.0	10.4

[a]Data provided by manufacturer; [b]Based on fibre outer diameter; [c]Data statistically determined using log-normal distribution; [d] [6],[e]Calculated using Eq. (1)., based on geometric pore shape coefficient, and in contact with an ammonia solution.

downstream [36,15]. However, clogging of the packed column following formation of crystalline NH_4HCO_3 has made the absorption-regeneration cycle difficult to manage [37]. Consequently, ammonia absorption studies generally advocate the elimination of crystalline ammonium bicarbonate formation during CO_2-NH_3 absorption [44,15].

Microporous hollow fibre membrane contactors (HFMC) can support the same overall chemical reaction between CO_2 and NH_3, but the introduction of a hydrophobic membrane is used to initiate indirect contact between gas and liquid phases. The CO_2 therefore freely diffuses from the gas phase on the lumen side, through the gas-filled pores of the membrane, and into an aqueous NH_3 liquid on the shell-side of the membrane [18]. Mediating the inclusion of CO_2 through the membrane, can improve governance over the rate of nucleation and crystal growth of ammonium bicarbonate [3]. Whilst the membrane introduces an additional resistance to mass transfer, the high specific surface area provides a process intensification 15 times greater than packed column technology [5]. McLeod et al. [27] also identified more than an order of magnitude reduction in NH_3 slip with HFMC. The authors attributed the reduced slip to the developed laminar flow in the liquid phase, as this constrains NH_3 transport *via* radial diffusion through the liquid film, stabilising NH_3 through chemical transformation to the non-gaseous protonated ammonium form (NH_4^+). Simple recovery of an aqueous NH_3 product from the gas-side of the membrane has also been proposed to further limit slip [40].

By decoupling gas and liquid phases, several authors have also successfully evidenced how a HFMC can permit formation of solid NH_4HCO_3 in the liquid phase following CO_2 absorption into NH_3 without causing membrane scaling [27,2,3]. The reduced mixing imposed by the characteristically laminar liquid phase, combined with a differential flow path across the interface, that is distinct from the gas phase, may also advantage solids transmission through the membrane. McLeod et al. [26] indicated how membrane hydrophobicity could benefit the induction of crystalline ammonium bicarbonate due to a reduction in activation energy for nucleation. This membrane also creates a unique concentration boundary layer at the three-phase line (gas-liquid-membrane) through the counter diffusion of CO_2 and NH_3, to create a supersaturated state which can control both nucleation and crystal growth. The crystal size distribution can be particularly important in this application, since this will govern the efficacy of transmission through the process, in addition to the kinetics of dissolution during regeneration of the solvent [2,3].

However, several studies have also identified crystalline ammonium bicarbonate primarily forming in the gas phase flowing through the membrane lumen following CO_2 absorption into NH_3 (Table 1) [24,26,9,40]. To illustrate, Makhloufi et al. [24] identified NH_4HCO_3 precipitation in the lumen-side (gas phase) which resulted in unstable CO_2 separation, gradually leading to process failure, and has been similarly observed by other authors [26,9]. Several mechanisms have been proposed which include: (i) a two-step wetting mechanism, in which the microporous membrane structure is wetted by the solvent, followed by breakthrough of aqueous NH_3 into the gas phase which quickly approaches sufficient supersaturation in the CO_2 rich gas phase to initiate nucleation [26]; (ii) a gas phase reaction between 'slipped' gaseous NH_3 and CO_2 to produce crystalline NH_4HCO_3; and (iii) a two-step condensation mechanism in which a binary water vapour/NH_3 mixture is co-transported from the solvent to the gas phase, before condensing and becoming rapidly supersaturated with sufficient CO_2 to initiate nucleation [26,40]. The probability for gas phase crystallisation is therefore dependent upon solvent chemistry (NH_3 concentration, reactant equilibria, fluid surface tension and temperature) which determines the rate and method of NH_3 transport into the gas phase, and the membrane properties (pore geometry, contact angle), which can enhance the probability for wetting and heterogeneous nucleation [26]. However, as each study applies different conditions, it is difficult to establish the extent to which each parameter contributes to the probability for inducing ammonium bicarbonate crystallisation and does not explain why some studies favour gas-phase crystallisation over liquid-phase crystallisation.

Delineating the mechanisms that can promote the crystallisation of ammonium bicarbonate preferentially within the liquid phase of a HFMC is therefore critically important in delivering sustainable NH_3-CO_2 absorption comprising consistent CO_2 separation, with the energetic benefit provided by formation of a solid phase NH_4HCO_3 reaction product. In this study, we therefore systematically explore critical process parameters that enable switching from lumen-side crystallisation to shell-side crystallisation, to sustain CO_2 separation by avoiding problematic gas phase reactions and improve recoverability of crystalline NH_4HCO_3 in the absorption solvent which could then be exploited to lower the energy barrier for solvent regeneration. The specific objectives are to: (i) determine the solvent conditions that primarily govern ammonia transport into the gas phase to prevent lumen side crystallisation; (ii) compare membranes of different properties to evidence how pore size and surface chemistry may promote lumen-side or shell-side crystallisation; and (iii) characterise reactant equilibria chemistry, nucleation kinetics and crystal growth phenomena to describe the mechanism underpinning preferential shell-side nucleation that can enable sustained recovery of crystalline NH_4HCO_3 in the solvent to promote low energy solvent regeneration.

2. Materials and methods

2.1. Fabrication, equipment setup and operation

The microporous PTFE hollow-fibre membrane comprised a nominal pore size of 0.18 μm (Zeus Industrial Products, Ireland). However, mono-axial stretching of the PTFE tube under heat, created an isotropic wall with oval pores of median length 4.5 μm (Table 2). The polypropylene hollow-fibre membrane comprised a nominal pore size of 0.2 μm, with a d_{max} of 0.36 μm indicating a more circular pore geometry

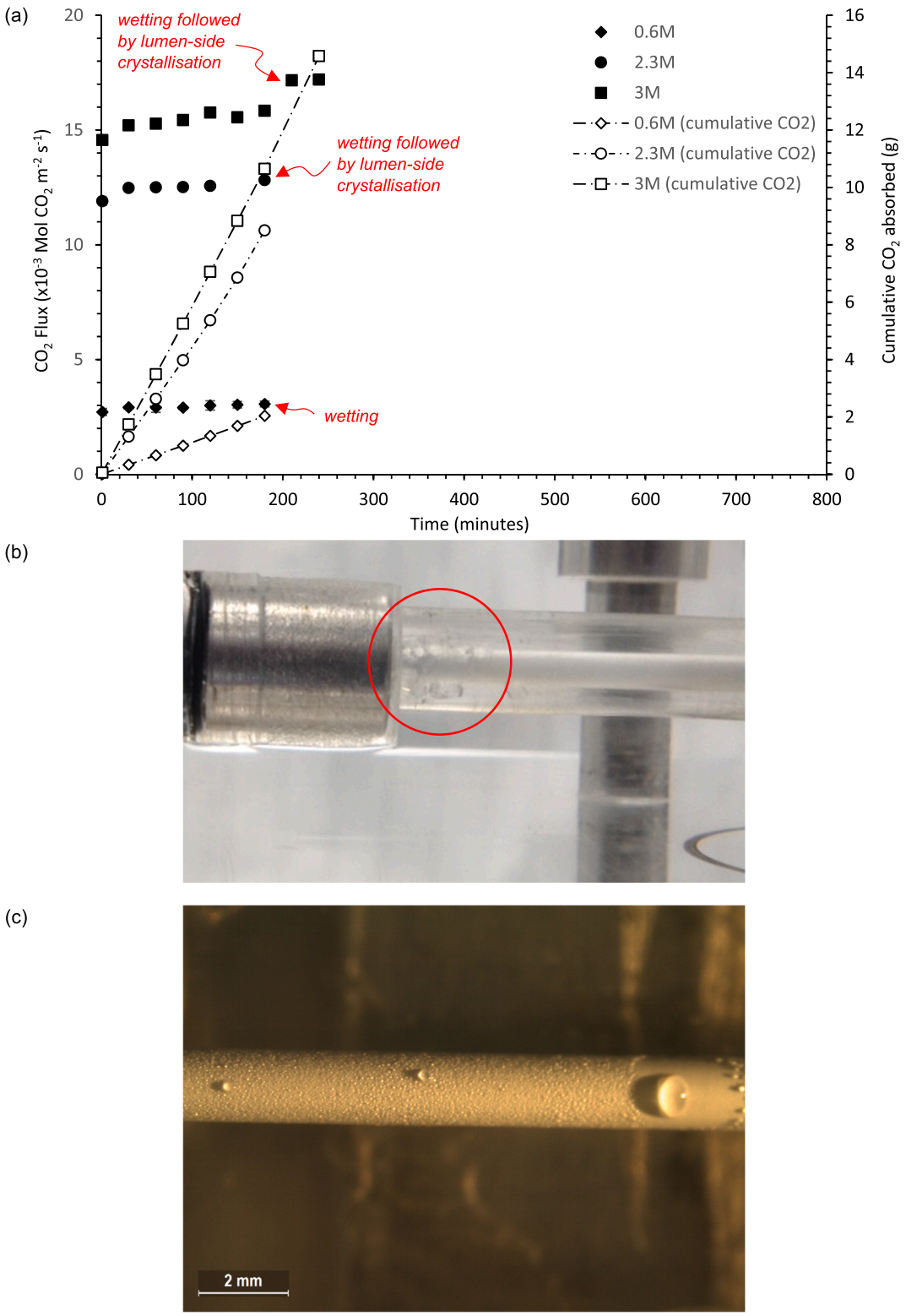

Fig. 1. (a) CO_2 absorption into ammonia concentration using for PTFE membrane, with absorbent in single pass. Conditions: G/L 11, V_G 0.2 m s^{-1}; V_L 1.4 × 10^{-3} m s^{-1}, temperature 20 °C. Error bars indicate standard deviation; (b) evidence of CO_2 bubbling at the solvent exit where is lower pressure drop exists; (c) close-up of CO_2 bubbling into the solvent on the shell-side of the fibre using direct visual observation for real time in-situ observation.

(Membrana GmbH, Wuppertal, Germany). Liquid entry pressure (Pa) was estimated according to [14]:

$$\Delta P_{B.P.} = \frac{-4B\gamma_L \cos\theta}{d_{max}} \quad (1)$$

where B (−) is the pore geometry coefficient, which takes a value between zero and unity (unity representing a perfectly spherical pore), γ_L(N m^{-1}) is the liquid surface tension, θ (°) is the contact angle at the membrane-liquid interface, d_{max} is the maximum pore length (m). For each experiment, single hollow-fibres were fixed into a Perspex cell (L,

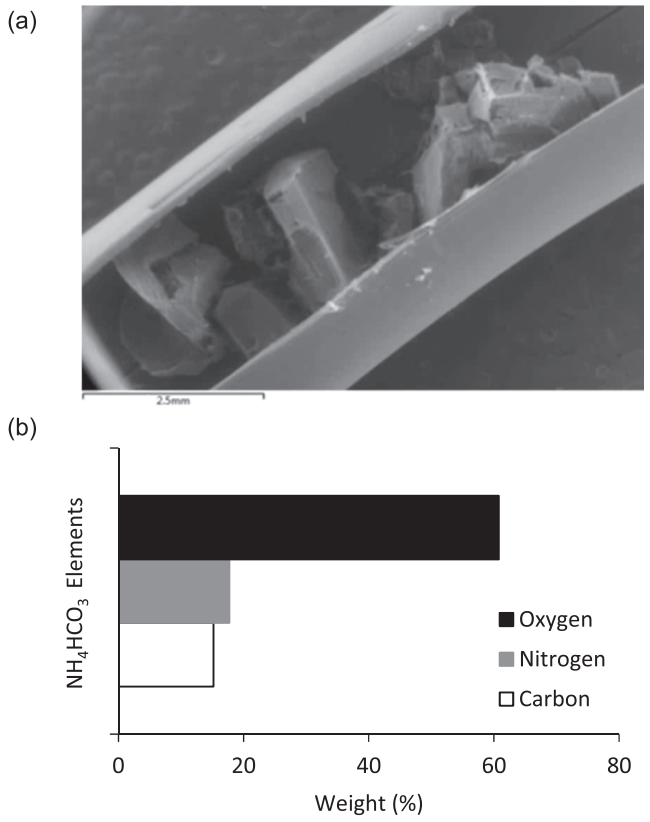

Fig. 2. Evidence of lumenside crystallisation following CO_2 absorption into aqueous ammonia, with absorbent in single pass: (a) SEM image of dissected hollowfibre showing crystals in lumen; (b) EDX analysis of lumen-side crystals indicating ammonium bicarbonate. Conditions: G/L 11, V_G 0.2 m s^{-1}; V_L 1.4 × 10^{-3} m s^{-1}, aqueous ammonia in single pass; absorbent temperature 20 °C.

165 mm) comprising a 12 mm diameter channel (Fig. 1). To permit direct observation on the shell-side of the membrane, a viewing window was engineered into the recess within the upper section of the cell. A stereomicroscope was fixed above the viewing window and images captured via high resolution camera (0.5x lens magnification; Nikon SMZ-2T, Milton Keynes, UK). Hollow-fibres were potted in epoxy resin (Bostick Ltd., Stafford, UK) and sealed into the crossflow cell. Pure CO_2 (99.8%, BOC gases, Ipswich, UK) was passed through the hollow-fibre lumen at a flow rate of 1000 ml min^{-1} using a laminar mass flow controller (0.01–1 L min^{-1}, Roxspur Measurement and Control Ltd., Sheffield, UK). Solvent was pumped counter-current on the shell-side of the membrane at 200 ml min^{-1} with a peristaltic pump (520Du, Watson-Marlow Ltd., Falmouth, UK). Solvent temperature (5 or 20 °C) was fixed with a refrigerated bath (R1 series, Grant Instruments Ltd., Cambridge, UK), and fluid temperatures monitored with K-type thermocouples (Thermosense Ltd., Bucks, UK). For further experimental details of setup, see Bavarella et al. [2,3].

2.2. Chemical preparation, sampling and analysis

Ammonia solvent was prepared by addition of aqueous NH_3 (35% Fisher Chemicals, Loughborough, UK) to de-ionised water (15.0 MΩ cm^{-1}). Solvent pH was fixed to pH 10 using hydrochloric acid (HCl, 37%, Fisher Scientific, Loughborough, UK), which has been commonly used in aqueous ammonia packed column processes [43], and ensures a high proportion of the ammonia solvent to be present in its deprotonated form (Fig. A1). Ammonia concentration was confirmed using ammonium cell test (VWR International Ltd., Poole, UK) followed by spectrophotometric determination (Spectroquant Nova 60, Merck-Millipore, Darnstadt, Germany). Gas flow rate was measured using manual volumetric flow meters of 50 and 1000 ml volume (Restek, Bellefonte, US; SKC, Blandford Forum, UK) to calculate the carbon dioxide flux (J_{CO2}, mol m^{-2} s^{-1}):

$$J_{CO_2} = \frac{\left(Q_{G,in} - Q_{G,out}\right) \times 273.15 \times 1000}{22.4 \times A_m T_G} \quad (2)$$

where $Q_{G,in}$ and $Q_{G,out}$ are gas flow rate (m^3 s^{-1}) before and after HFMC, A_m is the membrane surface area for absorption (m^2) and T_G is the gas temperature (K) [1]. The error for gas flow measurement was 2% of the reported value.

Solution pH was monitored using a Jenway epoxy bodied pH electrode (bulb end type) connected to a pH meter (Jenway 4330, Cole-Parmer, Stone, UK). The solution UV absorbance was determined at 215 nm (Jenway 6715 UV/Vis. Spectrophotometer, Cole-Parmer, Stone, UK) as this corresponds to the absorption of ammonium bicarbonate [42]. To characterise the development of the crystalline solid phase, experiments were terminated at different levels of supersaturation (C/C*), which was defined as the ratio between the CO_2 absorbed into solution that has transformed into bicarbonate and the CO_2 required to form ammonium bicarbonate at the solubility limit. For each level of supersaturation, sacrificial experiments were undertaken in triplicate and the crystal size distribution (CSD) determined. The solvent was initially filtered through a 0.45 μm Whatman filter and weighed (Camlab Ltd., Cambridge, UK). Crystals were then immersed in anhydrous alcohol to minimise agglomeration during counting [39] and transferred to a Sedgewick Rafter counting cell (S52 glass; Pyser-SGI, Edenbridge, Kent, UK) consisting of a 1 mm grid for counting under an optical microscope (Optech Microscope Services Ltd., Thame, UK). The microscope was equipped with a PL 5/0.12 lens and images captured using a digital camera (Infinity 3, Lumenera, Ottawa, Canada) linked to image processing software (Image Pro Plus, Media Cybernetics, Cambridge, UK) for CSD determination. Around 50 crystals were analysed from each image. For each sacrificial test, at least 600 crystals were classified to achieve sufficient accuracy for the CSD [19], which was determined assuming a log-normal distribution [20].

2.3. Chemistry of the NH_3-CO_2-H_2O system

Wang et al. [41] described the reaction between NH_3(aq) and CO_2(aq), including their equilibria dependent species, and the reversible reactions of ammonium carbamate/ carbamic acid formation:

$$CO_2(aq) + H_2O \underset{k_{-1}}{\overset{k_1}{\rightleftarrows}} H_2CO_3 \quad (3)$$

$$CO_2(aq) + OH^- \underset{k_{-2}}{\overset{k_2}{\rightleftarrows}} HCO_3^- \quad (4)$$

$$CO_3^{2-} + H^+ \underset{k_{-3}}{\overset{k_3}{\rightleftarrows}} HCO_3^- \quad (5)$$

$$HCO_3^- + H^+ \underset{k_{-4}}{\overset{k_4}{\rightleftarrows}} H_2CO_3 \quad (6)$$

$$OH^- + H^+ \underset{k_{-5}}{\overset{k_5}{\rightleftarrows}} H_2O \quad (7)$$

$$NH_3 + H^+ \underset{k_{-6}}{\overset{k_6}{\rightleftarrows}} NH_4^+ \quad (8)$$

The relative fraction of dissolved CO_2 and ammonia as carbonic acid (H_2CO_3) and protonated ammonium (NH_4^+) respectively, are dependent on solution pH and temperature (Fig. A1). The formation of carbamate as an intermediate product of reaction, and its protonation to carbamic

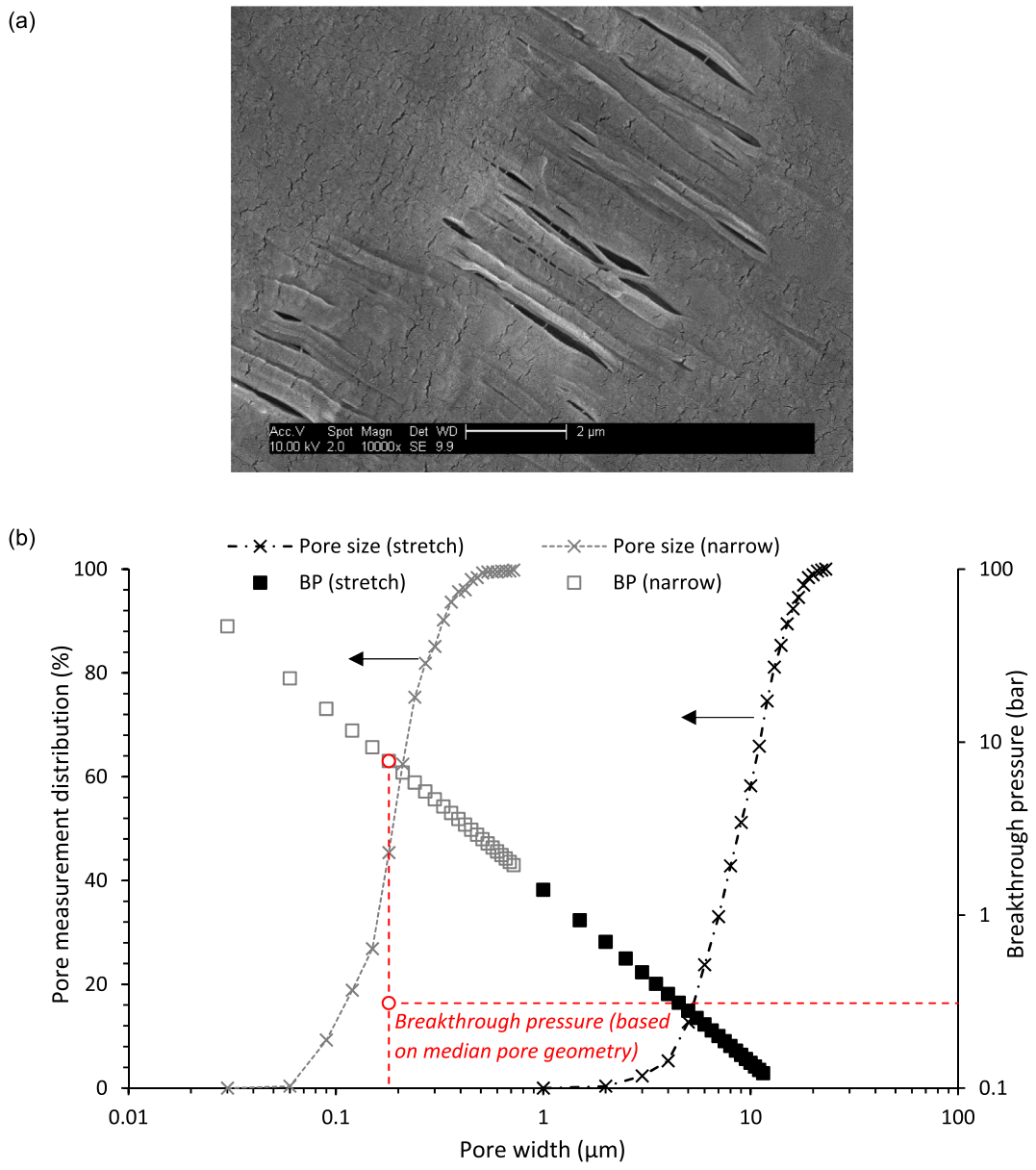

Fig. 3. (a) Pore structure of the PTFE membrane created through monoaxial stretching using SEM (10 k magnification; 10 kV AccV); (b) Pore size measurements of pore geometry (width and length of stretched pores), and their projected breakthrough pressures based on individual pore size measurements (secondary y-axis), and when median data are combined to form a median geometric shape factor coefficient (lower red circle).

acid are described by:

$$CO_2(aq) + NH_3 \underset{k_{-7}}{\overset{k_7}{\rightleftarrows}} NH_2COOH \tag{9}$$

$$NH_2CO_2^- + H^+ \underset{k_{-8}}{\overset{k_8}{\rightleftarrows}} NH_2COOH \tag{10}$$

Ammonium bicarbonate is formed from the ionic bond between NH_4^+ and HCO_3^- [29], which implies an equilibria dependency for the transformation of ammonia and carbon dioxide into crystalline ammonium bicarbonate (NH_4HCO_3):

$$NH_4^+(l) + HCO_3^-(l) \underset{k_{-9}}{\overset{k_9}{\rightleftarrows}} NH_4HCO_3(s) \tag{11}$$

Carbon dioxide and ammonia can produce ammonium carbamate (NH_2COONH_4) in the gas phase, or following reaction between the dissolved gases when in their nascent state:

$$CO_2(g) + 2NH_3(g) \underset{k_{-10}}{\overset{k_{10}}{\rightleftarrows}} NH_2COONH_4(s/l) \tag{12}$$

Through hydrolysis, NH_2COONH_4 successively converts into ammonium bicarbonate (NH_4HCO_3) [21]:

$$NH_2COONH_4(s) + CO_2(g) + H_2O(\underset{l}{g}) \underset{k_{-11}}{\overset{k_{11}}{\rightleftarrows}} 2NH_4HCO_3(s) \tag{13}$$

However, due to the high solubility of ammonium carbamate in water [23], ammonium bicarbonate formation in the gas phase is more likely to proceed by [21,16]:

$$CO_2(g) + NH_3(g) + H_2O(\underset{l}{g}) \underset{k_{-12}}{\overset{k_{12}}{\rightleftarrows}} NH_4HCO_3(s) \tag{14}$$

In total, five solid products can form, however, NH_4HCO_3 is

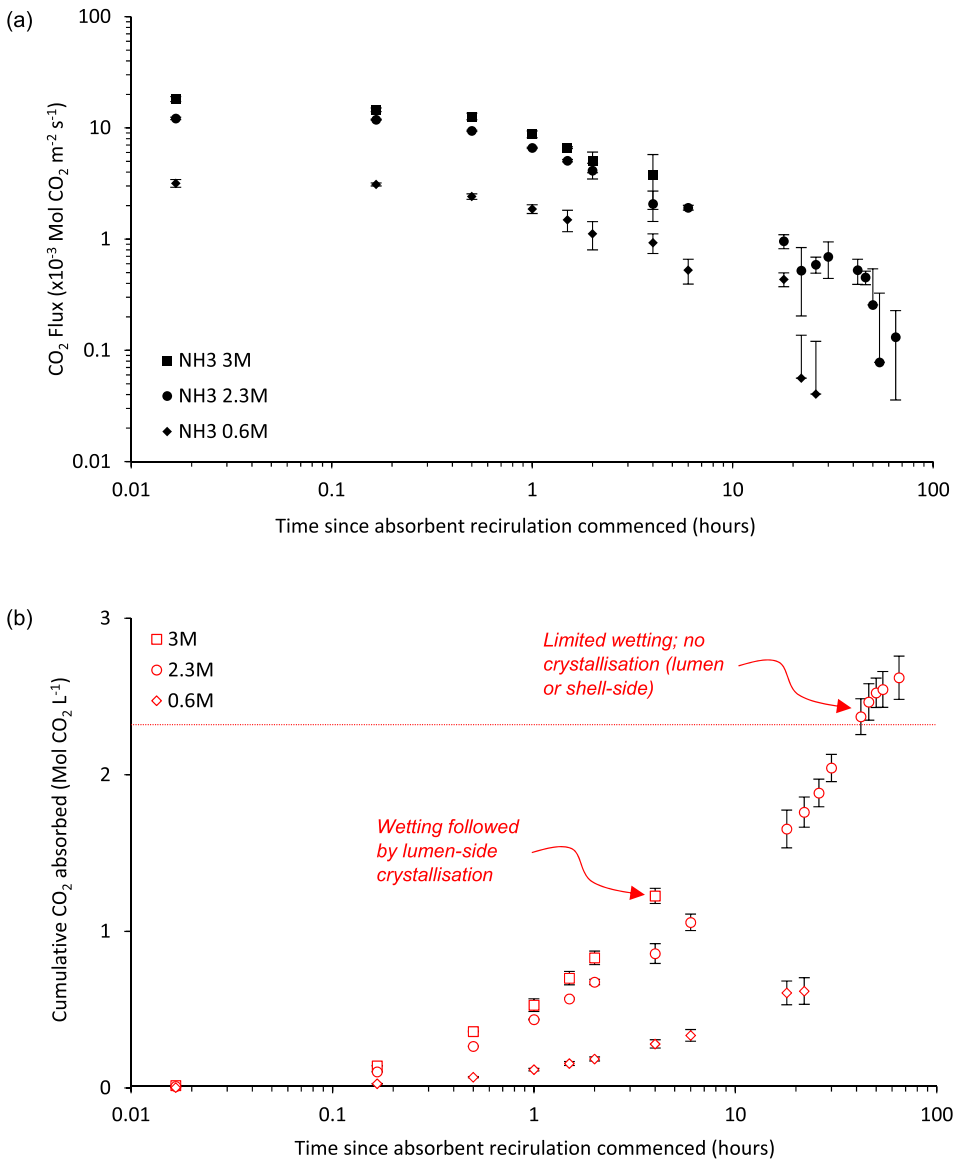

Fig. 4. Impact of recycling ammonia absorbent on wetting and lumen side crystallisation (observed immediately after wetting, t + 1) for PTFE membrane. Cumulative carbonate ratio compares CO_2 absorbed to HCO_3 concentration at saturation. Conditions: G/L 11, V_G 0.2 m s^{-1}, V_L 1.4 × 10^{-3} m s^{-1}, gas and absorbent temperature, 20 °C. Error bars indicate standard deviation. Red line indicates ammonium bicarbonate solubility at 20 °C.

thermodynamically favoured due to the lower solubility of the salt [23], which exhibits slight solubility-temperature dependency (Fig. B1a). Solvent temperature and concentration may also influence the probability for gas-side or liquid side NH_4HCO_3 crystallisation as this will determine the ammonia vapour pressure (Fig. B1b; [30].

3. Results and discussion

3.1. Creating baseline conditions to evaluate the probability for lumen side crystallisation

Initial experiments were undertaken with a PTFE membrane using conditions from the literature in which lumen side (gas phase) crystallisation was observed (solvent temperature 20 °C, NH_3 0.6–3 M; Table 1). A blockage in the lumen was first identified for each ammonia concentration by either a progressive increase in CO_2 flux, which was an artefact of the reduction in gas flow caused by the blockage (see 3 M NH_3, Fig. 1), or a complete interruption of gas flow [26]. Dindore et al. [11] described how for a liquid having intermediate surface tension, the liquid phase pressure drop over the fibre results in a higher inlet pressure, which could encourage localised wetting, and a lower pressure at the outlet, which could conversely introduce bubbling of the gas phase into the liquid phase near the outlet. In this study, an analogous observation was made following disruption to the gas flow, where CO_2 bubbling into the liquid was subsequently observed in the region of the fibre closest to the liquid outlet where the lowest pressure difference exists (Fig. 1b and 1c). Dissection of the hollow fibre membranes following operation, evidenced crystallisation to have proceeded within the lumen for the 2.3 and 3 M solvent concentrations (Fig. 2). While this did not occur for the lowest solvent concentration, CO_2 bubbling was coincident with observation of solvent droplets at the outlet of the lumen-side, indicating the presence of solvent in the gas phase for all three ammonia concentrations. Based on an estimation of the change in transmembrane pressure required to induce CO_2 breakthrough using the Hagen-Poiseuille equation [11], suggests that the partial filling of the lumen by the solvent may be sufficient to induce the back pressure needed to initiate bubbling without the onset of crystallisation.

Despite considerable differences in reactivity between NH_3 solvents,

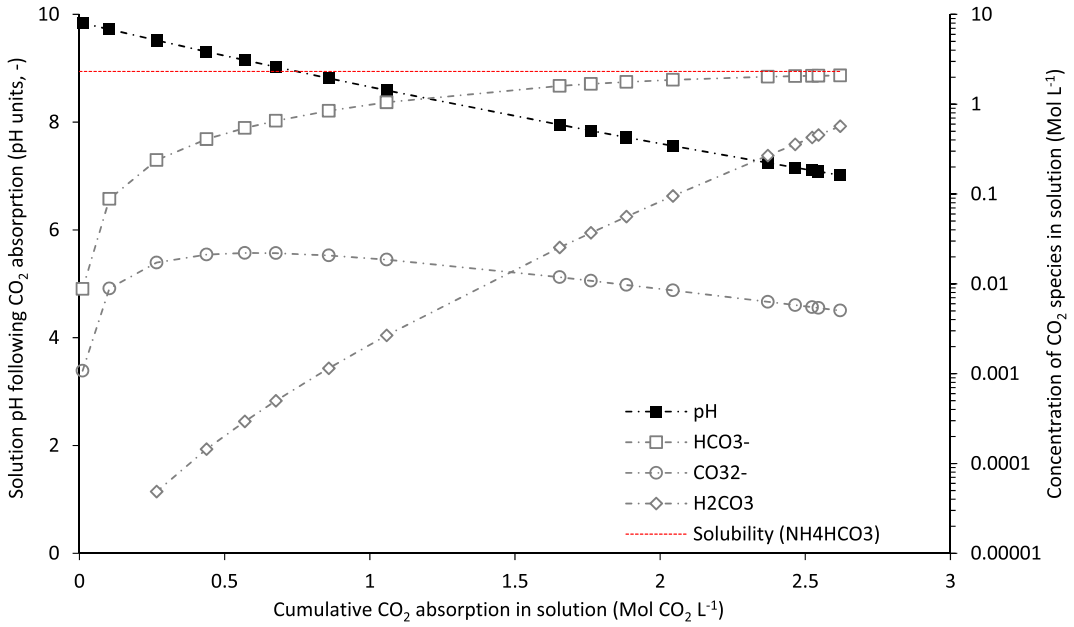

Fig. 5. Dynamic equilibria following progressive CO_2 absorption into 2.3 M aqueous ammonia in recirculation. Absorbent temperature 20 °C. Red line indicates ammonium bicarbonate solubility at 20 °C.

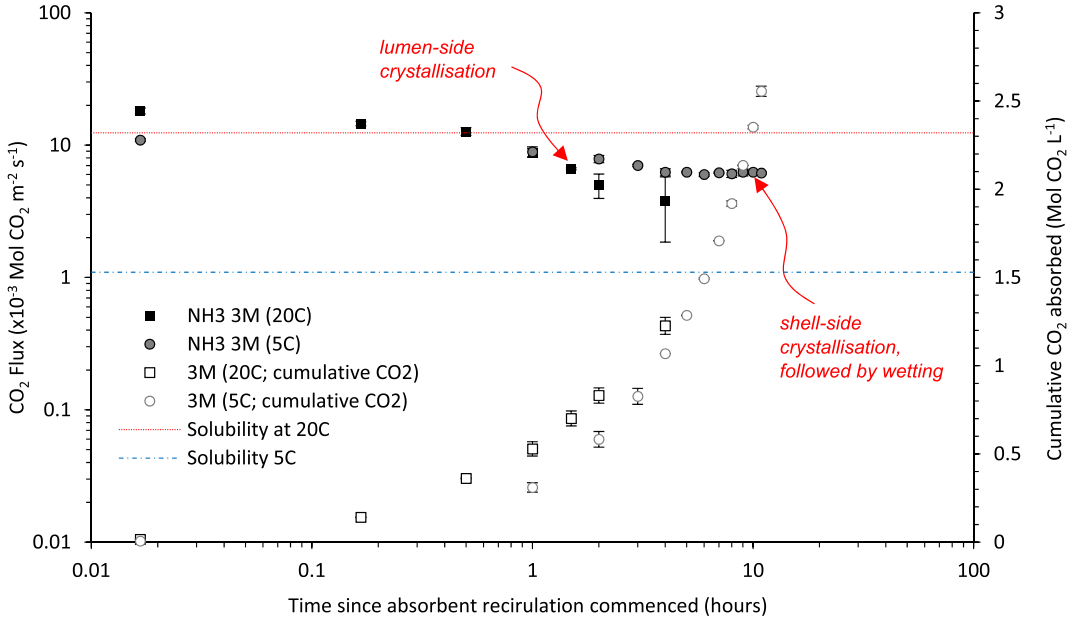

Fig. 6. Effect of absorbent temperature (3 M L^{-1} NH_3 in recirculation) on reactive membrane crystallisation. Cumulative carbonate ratio compares CO_2 absorbed to HCO_3 concentration at saturation. Conditions: PTFE membrane (μm pore size). Error bars indicate standard deviation. Horizontal lines indicates ammonium bicarbonate solubility at 20 °C (red) and 5 °C (blue).

CO_2 bubbling into the solvent was observed at similar times following operation, between 180 and 210 min (Fig. 1). The relative similarity in time to CO_2 breakthrough may therefore indicate that the physical mechanism of pore wetting by the ammonia solvent precedes lumen-side (gas-phase) crystallisation in a two-step process [26]. The difference in surface tension between ammonia solvents of less than 5 mN m^{-1} suggests that solvent breakthrough would not be strongly related to NH_3 concentration. However, due to the monoaxial stretching of PTFE during manufacturing, the pore structure comprised a narrow 'width' and stretched 'length' (Fig. 3). Measurement of over 500 pores, indicated the narrow dimension of the pores to range between 0.06 and 0.72 μm, with a median pore width of 0.18 μm, while the stretched pore dimension ranged between 1 and 11.5 μm, with a median pore length of 4.5 μm. Franken et al. [14] introduced the significance of the pore geometry to the induction of wetting. In this study, the median pore size data indicates a reduction in breakthrough pressure from approximately 7 bar (for spherical geometry) to less than 0.3 bar based on the *median* geometric pore shape coefficient. Dindore et al. [11] described how partial wetting proceeded by first wetting the larger pores in the pore size distribution. Since the PTFE membrane pore size distribution comprises of pores that are considerably greater than the median, the minimum breakthrough pressure will be noticeably below this value, implying a reasonable probability for wetting.

The cumulative absorption of 2, 8.5 and 15 gCO_2 was achieved at the

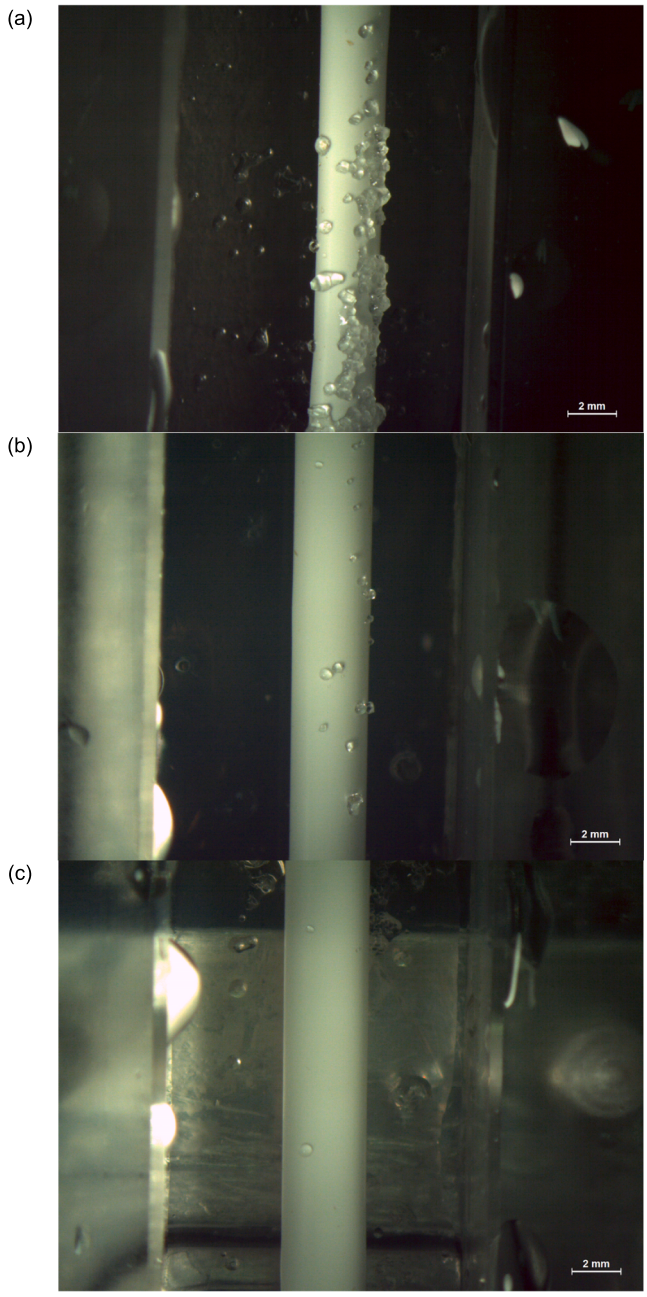

Fig. 7. Evidence for shell-side crystal nucleation using PTFE membrane using direct observation technique: (a) gas inlet (lumen), and aquaous ammonia outlet (shellside); (b) centre point of fibre; and (c) gas outlet (lumen) and aqueous ammonia inlet (shellside). Pore size, d_{max} 3.4 μm; initial ammonia concentration, 3 M; liquid temperature, 5 °C.

onset of CO_2 bubbling for ammonia solvent concentrations of 0.6, 2.3 and 3 M respectively (Fig. 1). As the solvent was operated in single pass, the volumetric concentration of CO_2 in the ammonia solvent was considerably below the concentration required to initiate crystallisation (ammonium bicarbonate saturation concentration (C*) 2.32 M, or a minimum of 102 g CO_2 L^{-1} at 20 °C)[2], which would indicate that crystallisation observed within the gas phase was independent of the liquid phase reaction. This is comparable to previous observations of CO_2-NH_3 absorption during single pass solvent flow [24,9,40]. For crystallisation to proceed in the gas phase, sufficient supersaturation must be achieved to overcome the energy barrier for nucleation [3]. As crystallisation in the gas phase was observed for the 2.3 M NH_3 solvent at 20 °C (Fig. 2), which is below the NH_3 concentration required to initiate nucleation in the solvent, gas phase crystallisation cannot be solely dependent on wetting occurring prior to nucleation. Instead, to overcome the energy barrier for nucleation, the ammonia concentration in the lumen must exceed the volumetric ammonia concentration within this solvent, which can only be achieved by the selective transport of ammonia gas across the membrane from the liquid phase to the gas phase. Several authors have suggested that if a crystalline product is formed through a gas phase reaction (Eq. (12)) [21,16], an ammonium carbamate (NH_2COONH_4) solid may be preferentially formed, as the reactants are less dependent on their respective equilibria. However, EDX analysis of the crystalline deposit in the lumen (Fig. 2b) exhibited a comparable C/N/O ratio to ammonium bicarbonate, which was confirmed by XRD[2]. We propose that this is thermodynamically favoured due to the lower solubility product of the bicarbonate salt, though its formation is equilibria dependent and thus requires sufficient water (in liquid or gas phase, Eq. (13) and (14)) to proceed[4]. This baseline analysis therefore emphasises that in addition to the role of pore structure in mediating the transmission of ammonia solvent from the liquid phase to the gas phase, NH_3 vapour pressure may also be critical to initiating gas phase crystallisation which is dependent on the solvent concentration, solvent temperature, and solvent reactivity, as they collectively govern the probability for selective (independent) NH_3 gas transport from the liquid phase to the gas phase.

3.2. Solvent reactivity is a critical factor in limiting gas phase crystallisation reactions

At full-scale, crystalline ammonium bicarbonate will form in the solvent along the length of the membrane contactor, as CO_2 absorbed in the solvent quickly reacts with NH_3 to produce carbamic acid. This is part of an equilibrium dependent reaction that will determine reactivity and is the step preceding nucleation (Eq. (9) and (10)), where formation of solid NH_4HCO_3 may therefore also limit NH_3 slip into the gas phase [15,2]. To evaluate whether this mechanism helps shift crystallisation from lumen side (gas phase) to shell-side (solvent), solvent recirculation was employed to mimic analogous conditions. Initial CO_2 flux was highest for the 3 M NH_3 solvent, while all three solvents exhibited a similar decline in CO_2 flux following solvent recirculation due to the decline in reactivity as NH_3 was progressively consumed through reaction (Fig. 4).

Blockage of the lumen by wetting or crystallisation was not observed for the 0.6 and 2.3 M solvents following recirculation (Fig. 4), despite the membrane having been in contact with the solvent for longer than in single pass, which supports the hypothesis that wetting is not the sole criteria governing gas phase crystallisation (Fig. 1). During the progressive absorption of CO_2, carbamic acid forms through the reaction between NH_3 and CO_2. The carbamic acid liberates [H^+] to reduce the solvent pH, shifting the ammonia-ammonium equilibrium from NH_3 to non-gaseous NH_4^+ [2](Fig. 5). This indirectly reduces the solvent ammonia vapour pressure, lowering the transmission of reactive NH_3 into the gas phase. By avoiding gas-phase blockages, prolonged CO_2 absorption was achieved, where the cumulative mass of CO_2 absorbed into the 2.3 M NH_3 solvent through recirculation was sufficient to theoretically achieve supersaturation (Fig. 4b). To illustrate, based on the ratio between the CO_2 absorbed (C, mol) and the CO_2 required to initiate nucleation (C*, mol of CO_2 in NH_4HCO_3 at saturation, 2.32 M L^{-1} at 20 °C), solvent supersaturation (C/C*) just exceeded 1. However, nucleation in the solvent was not observed. This can be explained by a shift in the carbonate equilibrium from HCO_3^- toward H_2CO_3 following acidification of the solvent, which reduced the actual NH_4HCO_3 solvent concentration to 2.05 M L^{-1} (88% of C/C*). This is below the concentration required to initiate shell-side (solvent) crystallisation (Fig. 5) and indicates that either a higher NH_3 solvent concentration or a reduction in solvent temperature (to reduce the solubility of NH_4HCO_3) is required to initiate shell-side crystallisation.

Lumen-side crystallisation was observed for the 3 M NH_3 solvent

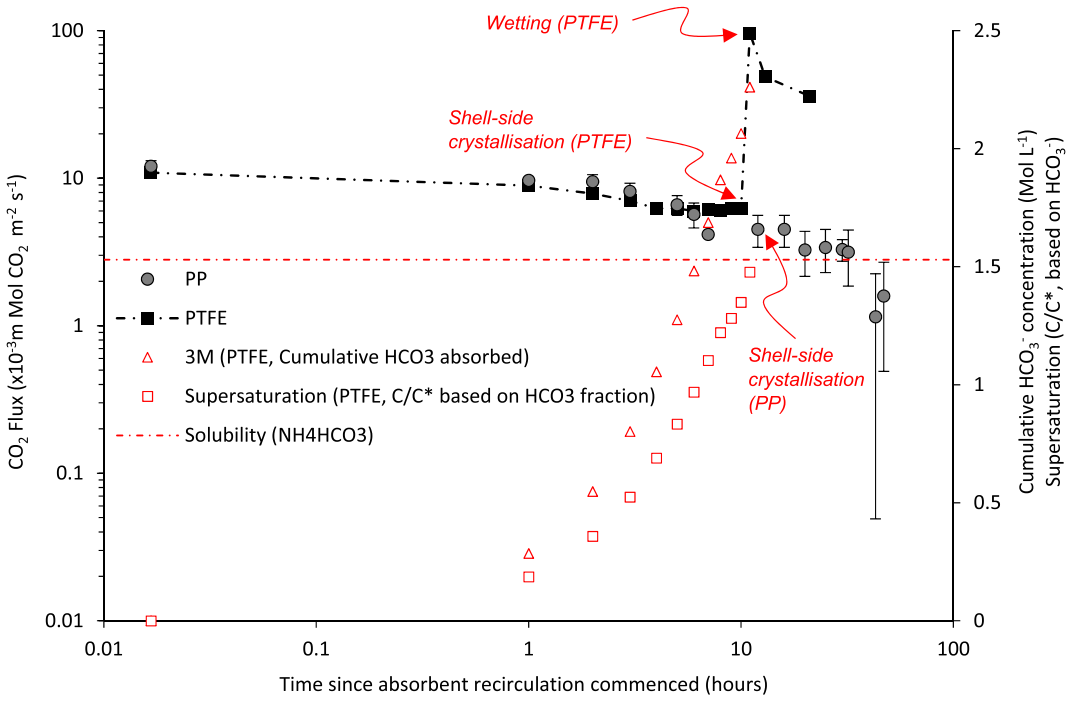

Fig. 8. Impact of membrane properties (PTFE, d_{max} 3.4 μm; PP, d_{max} 0.36 μm) on reactive membrane crystallisation. Absorbent HCO_3^- concentration and relative supersaturation (C/C*, based on HCO_3^- concentration; solubility, 1.53 mol NH_3 L^{-1} at 5 °C and 1 atm) illustrated for PTFE membrane. Conditions: Recirculating ammonia absorbent, 3 M; G/L 5. Error bars indicate standard deviation. Red line indicates ammonium bicarbonate solubility at 5 °C.

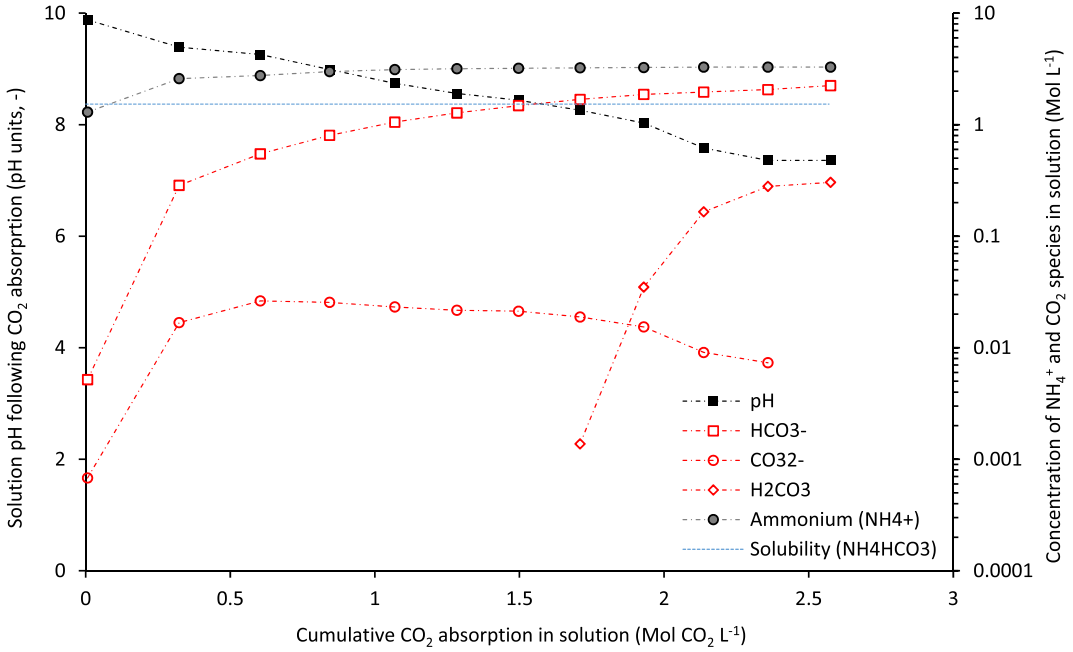

Fig. 9. Dynamic equilibria following progressive CO_2 absorption into 3 M aqueous ammonia in recirculation. Absorbent temperature 5 °C. Blue line indicates ammonium bicarbonate solubility at 5 °C.

after 4 h, which is only slightly longer than when operated in single pass (Fig. 4). This was coincident with a solvent CO_2 saturation concentration of C/C* 0.54, which is insufficient to initiate shell-side crystallisation. At the same solvent temperature, the NH_3 vapour pressure at 3 M is 65% higher than at 2.3 M (Appendix B, Fig. B1) [30]. Consequently, higher NH_3 transport from the solvent to the gas phase (slip) can be expected at the outset of solvent recirculation, where the unreacted nitrogen is primarily available in the NH_3 (gaseous) form. These observations are supported by McLeod et al. [26] noting lumen side (gas-phase) crystallisation to occur at solvent concentrations for 3 to 5 M but not at 2 M (Table 1). This analysis therefore implies that by reducing ammonia vapour pressure, the probability for gas-phase crystallisation can be reduced.

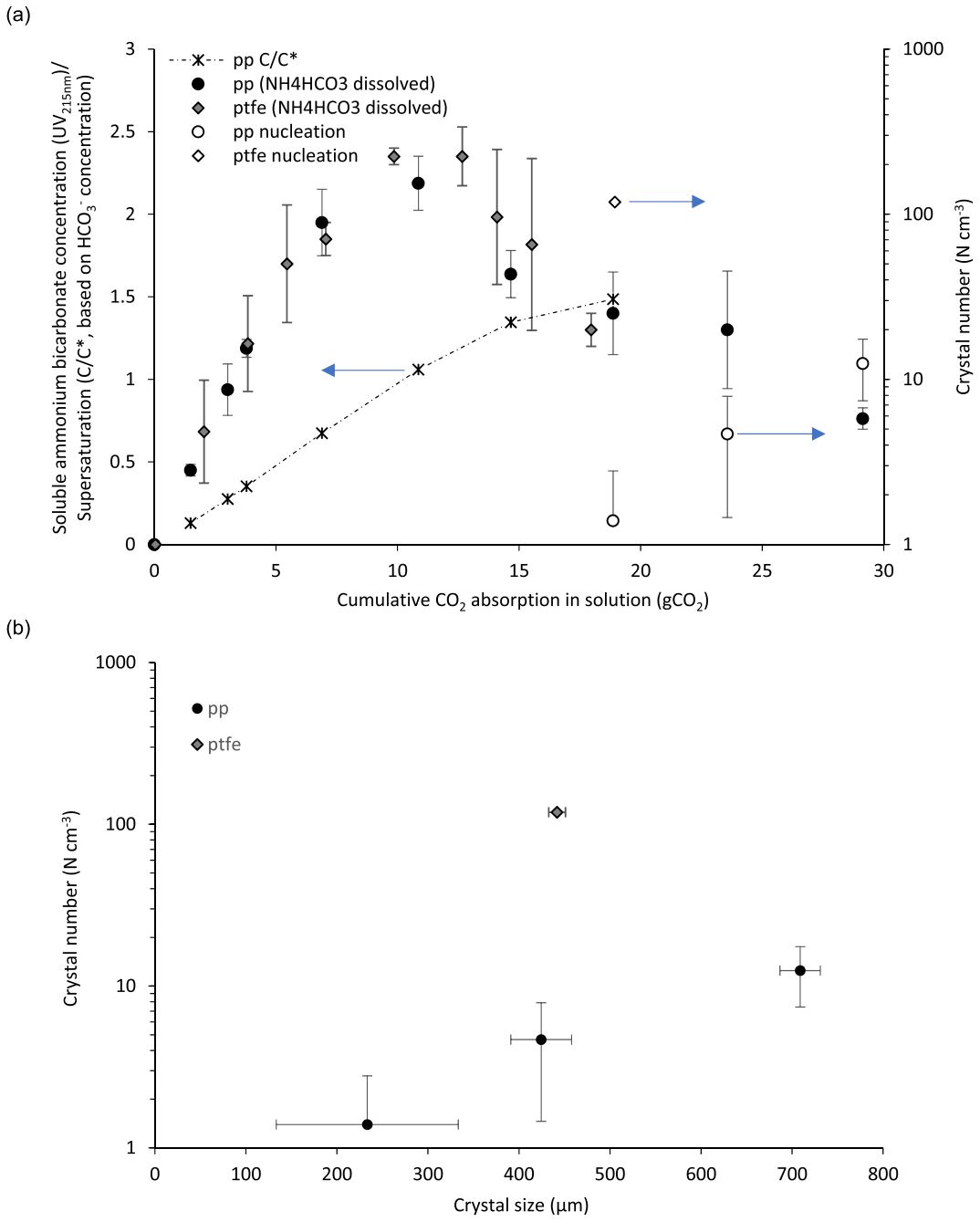

Fig. 10. Impact of membrane properties (PTFE, 3.4 µm; PP, 0.36 µm) on reactive membrane crystallisation: (a) crystal number; (b) median crystal size versus crystal number. Conditions: 3 M aqueous ammonia in recirculation; absorbent temperature 5 °C. Ammonium bicarbonate peak corresponds to minima in HCO_3^- and CO_3^{2-}, and is coincident with HCO_3^- concentration needed for induction (C/C* 1, 1.53 mol NH_3 L^{-1} at 5 °C and 1 atm). Error bars indicate standard deviation obtained from sacrificial experiments carried out in triplicate.

3.3. Temperature reduces solvent vapour pressure to reduce gas phase crystallisation

To examine the role of vapour pressure on gas phase crystallisation (independent of solvent concentration), the temperature of a 3 M NH_3 solvent was reduced from 20 to 5 °C, which reduced the vapour pressure from 6.1 to 2.9 kPa [30]. This also has implications for shell-side crystallisation, since the reduction in temperature lowers the solubility limit for NH_4HCO_3 by 30%, which favours the onset of nucleation at lower CO_2 concentrations (Appendix B, Fig. B1). Initial CO_2 flux was slightly lower at 5 °C than at 20 °C which can be explained by the reduced reaction kinetics (Fig. 6) [45]. However, when operating at the lower solvent temperature, a more consistent CO_2 flux was sustained over a longer duration, resulting in a supersaturated solvent. Crystallisation was first observed on the shell-side in the 5 °C solvent at a theoretical C/C*of 1.34, corresponding to a CO_2/NH_3 loading of 0.78. In addition to crystals collected from the solvent, nucleation was coincident with crystal growth on the fibre which were identified through direct observation (Fig. 7). Crystals formed on the fibre section closest to the CO_2 inlet were of larger diameter and greater in number, indicating that the concentration boundary layer at the membrane-solution interface plays a role in mediating nucleation.

Wetting occurred soon after shell-side crystallisation in the 5 °C solvent, as evidenced by a reduction of gas flow at the outlet of the

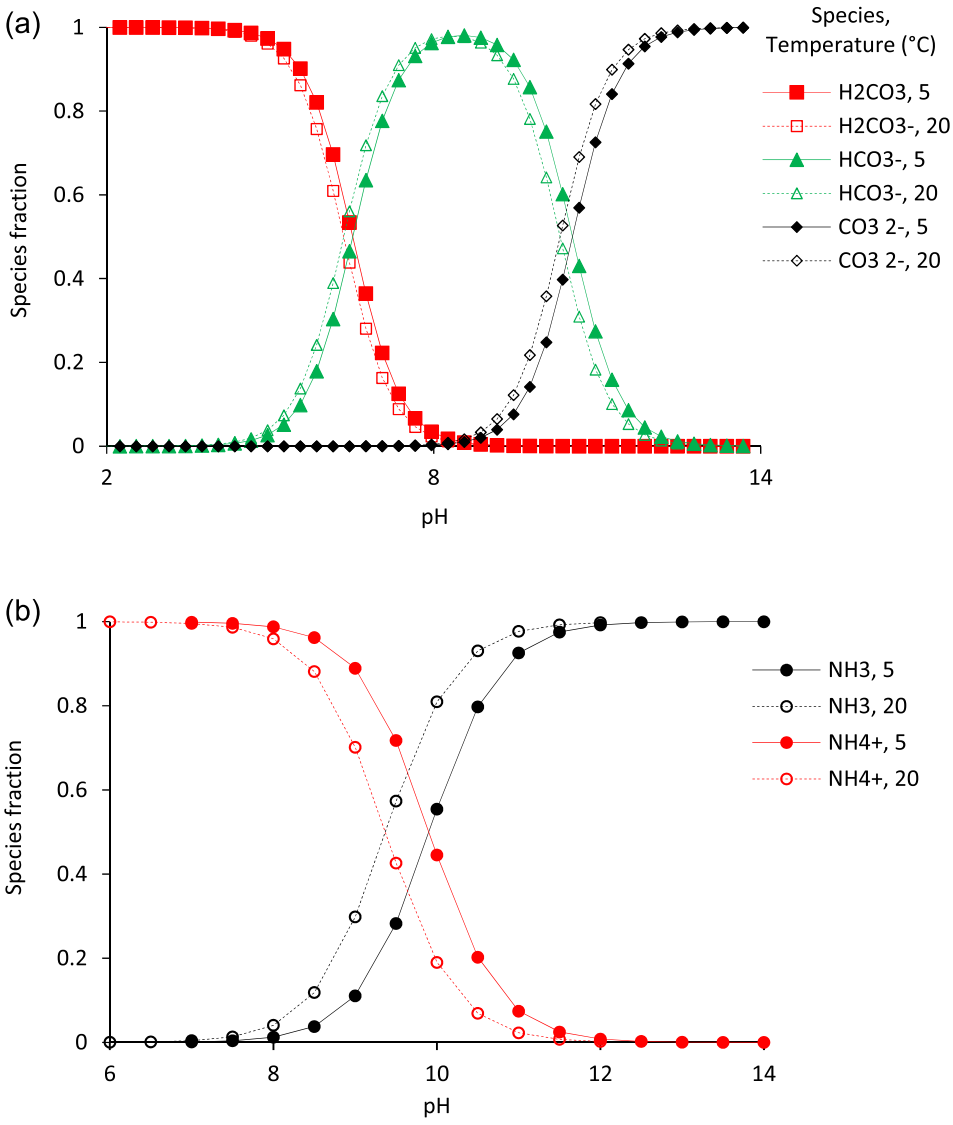

Fig. A1. Distribution of carbonic acid, bicarbonate and carbonate (H_2CO_3, HCO_3^-, CO_3^{2-}) (a) and of ammonium-ammonia (b) as functions of pH and solvent temperature.

lumen, and the bubbling of CO_2 into the liquid phase. This is in contradiction to observations at 20 °C where wetting was ostensibly followed by lumen-side crystallisation (Fig. 1). The membrane has been hypothesised to lower the activation energy for nucleation due to the interfacial energy of PTFE (contact angle, ~135°; [6], where the heterogeneous substrate can lower the level of supersaturation required for induction ($\Delta G_{het}/\Delta G_{hom}$, ~90%; [10]:

$$\frac{\Delta G_{het}}{\Delta G_{hom}} = 0.25(2+cos\theta)(1-cos\theta)^2\left[1-\varepsilon\frac{(1+cos\theta)^2}{(1-cos\theta)^2}\right]^3 \quad (16)$$

This expression has been adjusted to account for the membrane porosity (ε) which can also mediate local supersaturation in the region where the membrane (solid phase), liquid and gas phases intersect [26]. We propose that nucleation within the pores on the shell-side of the membrane for the 5 °C solvent subsequently alters the material contact angle, reducing the breakthrough pressure of the solvent which promotes pore wetting following shell-side crystallisation, leading to the transmission of solvent into the gas phase [34].

3.4. Tightening pore size to eliminate wetting after reactive membrane crystallisation occurs

A polypropylene (PP) hollow-fibre membrane was investigated within the same conditions to establish if a tighter pore size and sharper geometrical pore shape factor (B, from 0.15 to 0.56) could eliminate wetting following shell-side crystallisation, through providing 700% increase in breakthrough pressure (Table 2). Similar CO_2 flux profiles were initially observed for both membranes (Fig. 8). For the PTFE membrane, shell-side crystallisation proceeded once 2.36 M CO_2 L^{-1} were absorbed, equivalent to a supersaturation index (C/C*) of 1.34 based on bicarbonate speciation (2.06 M HCO_3^- L^{-1}; Fig. 9). For reference, shell-side crystallisation occurred soon after at a supersaturation index (C/C*) of between 1.34 and 1.48 for the PP membrane. Classical nucleation theory describes how nucleation rate is dependent upon the level of supersaturation [25]. Despite nucleation commencing at comparable levels of supersaturation, a higher nucleation rate was identified for the PTFE membrane, which recorded 118 # cm^{-3} (crystals/vol. of solvent) at C/C* of 1.48, compared to only 1.4 # cm^{-3} for the PP membrane at equivalent conditions (Fig. 10). This difference is not clearly explained by the interfacial energy of the two membrane substrates ($\Delta G_{het}/\Delta G_{hom}$, ~90% for PTFE and ~ 60% for PP), where the PP

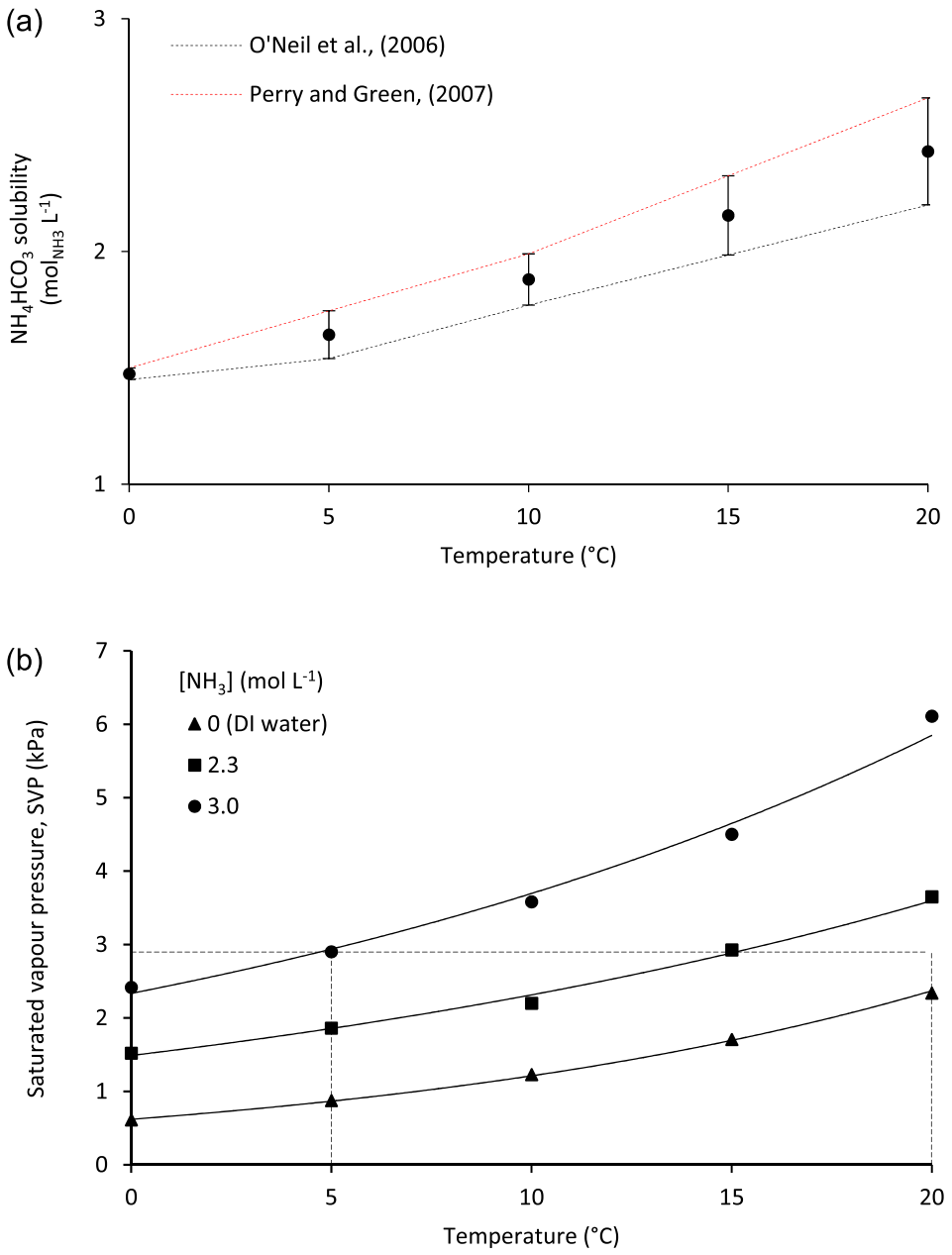

Fig. B1. (a) Ammonium bicarbonate (NH_4HCO_3) solubility in water. Symbols correspond to the mean calculated between experimental data from PubChem, [33] and Perry and Green, [31]; (b) Saturated vapour pressure of NH_3 over aqueous ammonia as a function of solution temperature. An increase in ammonia concentration or temperature increases the probability for ammonia slip.

polymer should foster greater reduction in activation energy to limit the supersaturation level required to initiate nucleation [13,6]. While the role of surface roughness cannot be discounted, a critical difference between the membranes is the coarse pore structure of the PTFE membrane, which we suggest can induce higher 'local fluxes', thereby raising the local supersaturation profile in the boundary layer, which can correlate to an increase in both nucleation and crystal growth [13]. While wetting soon followed shell-side crystallisation in the PTFE membrane, a stable CO_2 flux was observed in the PP membrane following primary nucleation, leading to the continuation of nucleation and growth (Fig. 10), which suggests that with the correct selection of pore size to mitigate wetting, solids formation can be promoted in membrane contactors to reduce the energy penalty for CO_2 separation.

4. Conclusions

In this study, the mechanism underpinning reactive crystallisation of ammonium bicarbonate is investigated as solids formation has previously led to process failure, while enabling its effective management could provide critical energy and cost benefits to solvent regeneration. The factors that are presumed to control crystallisation were characterised and used to decouple gas phase crystallisation from liquid phase crystallisation to permit the simultaneous separation of CO_2 with the recovery of an ammonium bicarbonate solid in the solvent. The following conclusions are drawn:

- While wetting was ostensibly observed before gas-phase crystallisation proceeded in the lumen, this was almost eliminated by reducing ammonia vapour pressure in the solvent. Therefore, it is NH_3 vapour transport which primarily governs induction in the gas-

phase. While beyond the scope of this present investigation, the water observed at the outlet of the lumen prior to gas-phase crystallisation could be due to condensation rather than wetting. Further work should consider how the chemical reaction shifts the gas phase concentration within the vapour-liquid-equilibrium for this ternary system, where the solvent developing in the gas phase could arise through an equilibrium dependent phase change (from vapour to liquid), and not simply mediated by capillary effect;

- Following solvent recirculation, the reduction in gas-phase crystallisation indicates how the shift in equilibria of the reactants following reaction, can dissipate the transmission of gaseous ammonia from the solvent to the gas phase. This mechanism helps to explain why ammonium bicarbonate solid formation can reduce ammonia slip as reported previously in mixed phase contactors, but also emphasises how the onset of nucleation in the solvent is dependent on the equilibrium;
- Increasing the solvent concentration can enhance supersaturation sufficient to overcome the activation energy for crystallisation in the solvent. However, increasing the solvent concentration raises the saturation vapour pressure of NH_3, leading to the risk of gas-phase reaction;
- Reducing solvent temperature limits the risk of gas-phase crystallisation, and lowers the supersaturation needed to initiate crystallisation in the solvent due to the change in solubility; however, we propose that it is the reduction in NH_3 vapour pressure which primarily supports the transition from lumen-side to shell-side nucleation;
- A narrow pore size distribution limits solvent entrapment that can lead to high nucleation rates, which can encourage wetting; creating a stable platform for the simultaneous separation and transformation of CO_2 to the solid phase.

The practical significance is that in resolving previous challenges experienced with solids formation in multiple reactor configurations (packed column, membrane contactors), the cost advantages of using an ammonia solvent can be realised, together with the energy saving for solvent regeneration, and exploited within hollow fibre membrane contactor geometry, which elicit a marked process intensification over conventional reactors. The outcomes can therefore contribute to driving down the cost of CCS which remains a critical barrier in the transition to net zero.

CRediT authorship contribution statement

S. Bavarella: Conceptualization, Data curation, Formal analysis, Investigation, Methodology, Writing – original draft. **B. Luqmani:** Data curation, Formal analysis, Writing – review & editing. **N. Thomas:** Data curation, Methodology, Writing – review & editing. **A. Brookes:** Conceptualization, Funding acquisition, Supervision. **A. Moore:** Conceptualization, Funding acquisition, Supervision. **P. Vale:** Conceptualization, Funding acquisition, Supervision. **M. Pidou:** Conceptualization, Funding acquisition, Supervision, Writing – review & editing. **E. J. McAdam:** Conceptualization, Data curation, Supervision, Funding acquisition, Project administration, Resources, Writing – review & editing.

Declaration of Competing Interest

The authors declare that they have no known competing financial interests or personal relationships that could have appeared to influence the work reported in this paper.

Acknowledgements

The authors would like to thank the Engineering and Physical Sciences Research Council for funding received via the STREAM CDT. The authors also thank Anglian Water, Northumbrian Water and Severn Trent Water for their financial support, as well as their contribution to shaping and delivering the research. Data underlying this paper can be accessed from: 10.17862/cranfield.rd.19291319.

References

[1] S. Atchariyawut, R. Jiraratananon, R. Wang, Separation of CO_2 from CH_4 by using gas–liquid membrane contacting process, J. Membr. Sci. 304 (1-2) (2007) 163–172.
[2] S. Bavarella, A. Brookes, A. Moore, P. Vale, G. Di Profio, E. Curcio, P. Hart, M. Pidou, E.J. McAdam, Chemically reactive membrane crystallisation reactor for CO2-NH3 absorption and ammonium bicarbonate crystallisation: Kinetics of heterogeneous crystal growth, J. Membr. Sci. 599 (2020) 117682, https://doi.org/10.1016/j.memsci.2019.117682.
[3] S. Bavarella, M. Hermassi, A. Brookes, A. Moore, P. Vale, G. Di Profio, E. Curcio, P. Hart, M. Pidou, E.J. McAdam, Is Chemically Reactive Membrane Crystallization Faciliated by Heterogeneous Primary Nucleation? Comparison with Conventional Gas-Liquid Crystallization for Ammonium Bicarbonate Precipitation in a CO_2-NH_3-H_2O System, Cryst. Growth Des. 20 (3) (2020) 1552–1564.
[4] S. Bavarella, M. Hermassi, A. Brookes, A. Moore, P. Vale, I.S. Moon, M. Pidou, E. J. McAdam, Recovery and concentration of ammonia from return liquor to promote enhanced CO_2 absorption and simultaneous ammonium bicarbonate crystallisation during biogas upgrading in a hollow fibre membrane contactor, Sep. Purif. Technol. 241 (2020), 116631.
[5] B. Belaissaoui, E. Favre, Novel dense skin hollow fiber membrane contactor based process for CO_2 removal from raw biogas using water as absorbent, Sep. Purif. Technol. 193 (2018) 112–126.
[6] F. Bougie, M.C. Iliuta, Analysis of Laplace-Young equation parameters and their influence on efficient CO_2 capture in membrane contactors, Sep. Purif. Technol. 118 (2013) 806–815.
[9] Z. Cui, D. deMontigny, Experimental study of carbon dioxide absorption into aqueous ammonia with a hollow fiber membrane contactor, J. Membr. Sci. 540 (2017) 297–306.
[10] E. Curcio, E. Fontananova, G. Di Profio, E. Drioli, Influence of the structural properties of poly(vinylidene fluoride) membranes on the heterogeneous nucleation rate of protein crystals, J. Phys. Chem. 110 (25) (2006) 12438–12445.
[11] V.Y. Dindore, D.W.F. Brilman, P.H.M. Feron, G.F. Versteeg, CO_2 absorption at elevated pressures using a hollow fibre membrane contactor, J. Mem. Sci. 235 (2005) 99–109.
[13] G. Di Profio, E. Curcio, E. Drioli, Supersaturation control and heterogeneous nucleation in membrane crystallizers: facts and perspectives, Ind. Eng. Chem. Res. 49 (23) (2010) 11878–11889.
[14] A.C.M. Franken, J.A.M. Nolten, M.H.V. Mulder, D. Bargeman, C.A. Smolders, Wetting criteria for the applicability of membrane distillation, J. Membr. Sci. 33 (3) (1987) 315–328.
[15] M. Gazzani, D. Sutter, M. Mazzotti, Improving the efficiency of a chilled ammonia CO_2 capture plant through solid formation: a thermodynamic analysis, Energy Proc. 63 (2014) 1084–1090.
[16] K. Han, C.K. Ahn, M.S. Lee, C.H. Rhee, J.Y. Kim, H.D. Chun, Current status and challenges of the ammonia-based CO_2 capture technologies toward commercialization, Int. J. Greenh. Gas Con. 14 (2013) 270–281.
[18] S. Heile, S. Rosenberger, A. Parker, B. Jefferson, E.J. McAdam, Establishing the suitability of symmetric ultrathin wall polydimethylsiloxane hollow-fibre membrane contactors for enhanced CO_2 separation during biogas upgrading, J. Membr. Sci. 452 (2014) 37–45.
[19] X. Ji, E. Curcio, S. Al Obaidani, G. Di Profio, E. Fontananova, E. Drioli, Membrane distillation-crystallization of seawater reverse osmosis brines, Sep. Purif. Technol. 71 (1) (2010) 76–82.
[20] K. Li, J. Kong, X. Tan, Design of hollow fibre membrane modules for soluble gas removal, Chem. Eng. Sci. 55 (2000) 5579–5588.
[21] X. Li, E. Hagaman, C. Tsouris, J.W. Lee, Removal of carbon dioxide from flue gas by ammonia carbonation in the gas phase, Energy Fuels 17 (1) (2003) 69–74.
[23] F. Mani, M. Peruzzini, P. Stoppioni, CO_2 absorption by aqueous NH_3 solutions: speciation of ammonium carbamate, bicarbonate and carbonate by a ^{13}C NMR study, Green Chem. 8 (11) (2006) 995, https://doi.org/10.1039/b602051h.
[24] C. Makhloufi, E. Lasseuguette, J.C. Remigy, B. Belaissaoui, D. Roizard, E. Favre, Ammonia based CO_2 capture process using hollow fiber membrane contactors, J. Membr. Sci. 455 (2014) 236–246.
[25] M.A. McDonald, H. Salami, P.R. Harris, C.E. Lagerman, X. Yang, A.S. Bommarius, M.A. Grover, R.W. Rousseau, Reactive crystallisation: a review, React. Chem. Eng. 6 (2021) 364–400.
[26] A. McLeod, P. Buzatu, O. Autin, B. Jefferson, E. McAdam, Controlling shell-side crystal nucleation in a gas–liquid membrane contactor for simultaneous ammonium bicarbonate recovery and biogas upgrading, J. Membr. Sci. 473 (2015) 146–156.
[27] A. McLeod, B. Jefferson, E.J. McAdam, Biogas upgrading by chemical absorption using ammonia rich absorbents derived from wastewater, Water Res. 67 (2014) 175–186.
[29] Z. Niu, Y. Guo, Q. Zeng, W. Lin, Experimental studies and rate-based process simulations of CO_2 absorption with aqueous ammonia solutions, Ind. Eng. Chem. Res. 51 (14) (2012) 5309–5319.
[30] E.P. Perman, Vapour pressure of aqueous ammonia solution. Part II, J. Chem. Soc. Trans. 83 (1903) 1168–1184.

[31] R.H. Perry, D.W. Green. Perry's Chemical Engineers' Handbook 8 (2007) 2–126.
[33] PubChem. U.S. National Library of Medicine, 2004. Retrieved from https://pubchem.ncbi.nlm.nih.gov/compound/ammonium_bicarbonate (accessed 17th November, 2021).
[34] H.A. Rangwala, Absorption of carbon dioxide into aqueous solutions using hollow fiber membrane contactors, J. Membr. Sci. 112 (2) (1996) 229–240.
[36] M.a. Shuangchen, S. Huihui, Z. Bin, C. Gongda, Experimental study on additives inhibiting ammonia escape in carbon capture process using ammonia method, Chem. Eng. Res. Des. 91 (12) (2013) 2775–2781.
[37] D. Sutter, M. Gazzani, M. Mazzotti, Formation of solids in ammonia-based CO_2 capture processes — Identification of criticalities through thermodynamic analysis of the CO_2–NH_3–H_2O system, Chem. Eng. Sci. 133 (2015) 170–180.
[38] M. Trypuć, U. Kiełkowska, Solubility in the NH_4HCO_3+$NaHCO_3$+H_2O System, J. Chem. Eng. Data 43 (2) (1998) 201–204.
[39] A.R. Veiga, C.E. Calmanovici, M. Giulietti. Operational conditions evaluation in ammonium bicarbonate crystallisation. Proceedings of the 14th International Symposium on Industrial Crystallization 65 (1999) 1−12.
[40] K. Villeneuve, D. Roizard, J.-C. Remigy, M. Iacono, S. Rode, CO_2 capture by aqueous ammonia with hollow fiber membrane contactors: Gas phase reactions and performance stability, Sep. Purif. Technol. 199 (2018) 189–197.
[41] X. Wang, W. Conway, D. Fernandes, G. Lawrance, R. Burns, G. Puxty, M. Maeder, Kinetics of the reversible reaction of CO_2 (aq) with ammonia in aqueous solution, J. Phys. Chem. A. 115 (24) (2011) 6405–6412.
[42] N.S. Wilson, R. Morrison, J.W. Dolan, Buffers and Baselines, LC-GC Europe. 1 (2001) 1–3.
[43] J.T. Yeh, K.P. Resnik, K. Rygle, H.W. Pennline, Semi-batch absorption and regeneration studies for CO_2 capture by aqueous ammonia, Fuel Process. Technol. 86 (14-15) (2005) 1533–1546.
[44] H. Yu, G. Qi, S. Wang, S. Morgan, A. Allport, A. Cottrell, T. Do, J. McGregor, L. Wardhaugh, P. Feron, Results from trialling aqueous ammonia-based post-combustion capture in a pilot plant at Munmorah Power Station: Gas purity and solid precipitation in the stripper, Int. J. Greenh. Gas Con. 10 (2012) 15–25.
[45] H. Yu, Z. Tan, J. Thé, X. Feng, E. Croiset, W.A. Anderson, Kinetics of the absorption of carbon dioxide into aqueous ammonia solutions, AlChE J. 62 (10) (2016) 3673–3684.

Further reading

[7] A. Capodaglio, P. Hlavinek, M. Raboni, Physico-chemical technologies for nitrogen removal from wastewaters: a review, Rev. Ambient. Agua 10 (2015) 482–493.
[8] L.-H. Cheng, P.-C. Wu, J. Chen, Modeling and optimization of hollow fiber DCMD module for desalination, J. Membr. Sci. 318 (1-2) (2008) 154–166.
[12] G.D. Profio, E. Curcio, A. Cassetta, D. Lamba, E. Drioli, Membrane crystallization of lysozyme: kinetic aspects, J. Cryst. Growth. 257 (3-4) (2003) 359–369.
[17] Q. He, G.e. Yu, T.e. Tu, S. Yan, Y. Zhang, S. Zhao, Closing CO_2 loop in biogas production: recycling ammonia as fertilizer, Environ. Sci. Technol. 51 (15) (2017) 8841–8850.
[22] J. Liu, S. Wang, B.o. Zhao, H. Tong, C. Chen, Absorption of carbon dioxide in aqueous ammonia, Energy Proc. 1 (1) (2009) 933–940.
[28] F. Millero, R.N. Roy, A Chemical Equilibrium Model for the Carbonate System in Natural Waters, Croat. Chem. Acta. 70 (1997) 1–38.
[32] M. Persson, O. Jonsson, A. Wellinger, Biogas upgrading to vehicle fuel standards and grid injection, IEA Bioenergy Task 37 (2006) 1–34.
[35] A. Read, F. Hofmann, Does biogas scrub up? Mater. Recycling World 2 (2011) 20–21.